The Astrophysical Journal Letters, 954:L10 (6pp), 2023 September 1 https://doi.org/10.3847/2041-8213/ace0c8

First Constraints on Dense Molecular Gas at $z = 7.5149$ from the Quasar Pōniuā'ena

Chiara Feruglio[1,2], Umberto Maio[1], Roberta Tripodi[1,2,3], Jan Martin Winters[4], Luca Zappacosta[5], Manuela Bischetti[1,3], Francesca Civano[6], Stefano Carniani[7], Valentina D'Odorico[1,2,7], Fabrizio Fiore[1,2], Simona Gallerani[7], Michele Ginolfi[8], Roberto Maiolino[9,10,11], Enrico Piconcelli[5], Rosa Valiante[5], and Maria Vittoria Zanchettin[1,12]

[1] INAF—Osservatorio Astronomico di Trieste, Via G. Tiepolo 11, I-34143 Trieste, Italy; chiara.feruglio@inaf.it
[2] IFPU—Institute for Fundamental Physics of the Universe, via Beirut 2, I-34151 Trieste, Italy
[3] Dipartimento di Fisica, Università di Trieste, Sezione di Astronomia, Via G.B. Tiepolo 11, I-34131 Trieste, Italy
[4] IRAM, 300 rue de la Piscine, Domaine Universitaire de Grenoble, F-38406 St.-Martin-d'Héres, France
[5] INAF—Osservatorio Astronomico di Roma, Via Frascati 33, I-00040 Monte Porzio Catone, Italy
[6] Astrophysics Science Division, NASA Goddard Space Flight Center, Greenbelt, MD 20771, USA
[7] Scuola Normale Superiore, Piazza dei Cavalieri 7 I-56126 Pisa, Italy
[8] Dipartimento di Fisica e Astronomia, Universita' di Firenze, Via G. Sansone 1, 50019 Sesto Fiorentino (Firenze), Italy
[9] Institute of Astronomy, University of Cambridge, Madingley Road, Cambridge CB3 0HA, UK
[10] Kavli Institute for Cosmology, University of Cambridge, Madingley Road, Cambridge CB3 0HA, UK
[11] Department of Physics and Astronomy, University College London, Gower Street, London WC1E 6BT, UK
[12] SISSA, Via Bonomea 265, I-34136 Trieste, Italy
Received 2023 April 17; revised 2023 June 6; accepted 2023 June 12; published 2023 August 29

Abstract

We report the detection of CO(6–5) and CO(7–6) and their underlying continua from the host galaxy of quasar J100758.264+211529.207 (Pōniuā'ena) at $z = 7.5149$, obtained with the NOrthern Extended Millimeter Array. Pōniuā'ena belongs to the HYPerluminous quasars at the Epoch of ReionizatION sample of 18 $z > 6$ quasars selected to be powered by supermassive black holes, which experienced the fastest mass growth in the first cosmic gigayear. The one reported here is the highest-redshift measurement of the cold and dense molecular gas to date. The host galaxy is unresolved, and the line luminosity implies a molecular reservoir of $M(H_2) = (2.2 \pm 0.2) \times 10^{10}$ $M_\odot$, assuming a CO spectral line energy distribution typical of high-redshift quasars and a conversion factor $\alpha = 0.8$ $M_\odot(\mathrm{K\ km\ s^{-1}\ pc^2})^{-1}$. We model the cold dust spectral energy distribution to derive a dust mass of $M_{\mathrm{dust}} = (1.7 \pm 0.6) \times 10^8$ $M_\odot$ and thus, a gas-to-dust ratio ∼130. Both the gas and dust mass are remarkably similar to the reservoirs found for luminous quasars at $z \sim 6$–7. We use the CO detection to derive an estimate of the cosmic mass density of H_2, $\Omega_{H_2} \simeq 1.31 \times 10^{-5}$. This value is in line with the general trend suggested by literature estimates at $z < 7$ and agrees fairly well with the latest theoretical expectations of nonequilibrium molecular-chemistry cosmological simulations of cold gas at early times.

Unified Astronomy Thesaurus concepts: Quasars (1319)

1. Introduction

Since the first $z > 6$ quasar discovery (Fan et al. 2001), the population of quasars near the Epoch of Reionization (EoR) has increased up to ∼300 sources, and the frontier of the quasar search has been pushed back to 0.7 Gyr with the recent discovery of eight $z > 7$ quasars. It is noteworthy that three of them are at $z \sim 7.5$, well inside the EoR (Bañados et al. 2018; Yang et al. 2020; Wang et al. 2021). These quasars are powered by supermassive black holes (SMBHs) with masses from $M_{\mathrm{BH}} = 10^8$ $M_\odot$ up to 10^{10} $M_\odot$, shining close to the Eddington limit, with bolometric luminosities at the brightest end of the quasar luminosity function, $L_{\mathrm{bol}} > 5 \times 10^{46}$ erg s^{-1} (Willott et al. 2010; Mazzucchelli et al. 2017; Onoue et al. 2019). At Far-IR/submillimeter wavelengths, observations reveal the presence of copious amounts of dust ($>10^8$ $M_\odot$), and star formation rates (SFRs) up to 1000–3000 $M_\odot$ yr^{-1}, within the host galaxies (e.g., Maiolino et al. 2005; Wang et al. 2013; Feruglio et al. 2018; Venemans et al. 2017, 2020), albeit with large systematic uncertainties (Tripodi et al. 2023).

The cold molecular phase is the least explored up to now at $z > 6$. A few tens of quasars at redshift up to $z \sim 6.8$ have been detected in carbon monoxide (CO) rotational transitions, which are the most direct tracers of the cold molecular interstellar medium (ISM), indicating massive molecular reservoirs of dense gas feeding both star formation and nuclear accretion (Wang et al. 2013, 2016; Gallerani et al. 2014; Carniani et al. 2019; Venemans et al. 2017; Decarli et al. 2022). The CO spectral line energy distributions (SLEDs) modeling indicate that in addition to the far-UV radiation from young and massive stars, another gas heating mechanism (e.g., X-ray radiation and/or shocks) may be needed to explain the observed CO luminosities (Li et al. 2020; Pensabene et al. 2021; Decarli et al. 2022). Only in a few cases it was possible to spatially resolve the molecular reservoirs and map disks or dispersion-dominated hosts (Walter et al. 2004, 2022; Feruglio et al. 2018; Yue et al. 2021; Shao et al. 2022). At $z > 7$, the dense molecular gas reservoirs have been investigated in only two quasars, J1342+0928 at $z = 7.54$ and J112001.48+064124.30 at $z = 7.08$, and remained so far undetected (Novak et al. 2019).

This Letter is part of a series of papers (currently including Tripodi et al. 2023; Zappacosta et al. 2023) dedicated to the HYPerluminous quasars the Epoch of ReionizatION

(HYPERION) sample. HYPERION consists of eighteen $z = 6 - 7.5$ luminous ($L_{\rm bol} \sim 10^{47.3}$ erg s^{-1}), highly accreting, and massive ($M_{\rm BH} = 10^9$–10^{10} $M_\odot$) quasars selected to be powered by SMBHs, which experienced the fastest mass growth in the first gigayear of the universe, and which are targets of a 2.4 Ms XMM-Newton Multi-Year Heritage program (Zappacosta et al. 2023). In this Letter we report the detection of CO(6–5) and (7–6) along with their underlying continua for the quasar J100758.264+211529.207 (dubbed Pōniuā'ena) at $z = 7.5419$, obtained with the NOrthern Extended Millimeter Array (NOEMA) in the framework of a multiwavelength follow-up of the HYPERION quasars. This quasar was first discovered by Yang et al. (2020) and is one of the three highest-redshift quasars known, all located at the midpoint of the Reionization Epoch, $z \sim 7.5$. The CO detections presented here enable the first estimate of the molecular gas reservoirs at these high redshifts and of the gas-to-dust-mass ratio. We adopt a ΛCDM cosmology with parameters $\Omega_\Lambda = 0.714$, $\Omega_m = 0.286$ and $H_0 = 69.6$ km s^{-1} Mpc^{-1}. At $z = 7.5149$, the age of the universe is 702 Myr, and the angular scale ∼5.11 kpc arcsec^{-1}.

2. Observations and Data Analysis

Observations were taken with the NOEMA interferometer under project W21ED in March 2022. The receivers were tuned at 81.2 GHz in the lower sideband (LSB). The CO(6–5) emission line from the quasar host galaxy is redshifted to the LSB, while the CO(7–6) line lies in the upper sideband (USB), so the bandwidth covered by the correlator PolyFiX enables detection of both lines in a single frequency tuning. Amplitude and phase calibration were done on the quasars J1012+232 and J0953+254, and LkHa101 (0.2 Jy) was used as flux calibrator. Calibration and imaging was performed using CLIC and MAPPING within the GILDAS software.[13]

The continuum visibility tables at two representative frequencies in LSB and USB were derived using the task uv_filter within MAPPING to filter out a spectral region 400 MHz wide around the emission lines, and uv_continuum. The noise reaches 15.5 μJy beam^{-1} in LSB and 13.7 μJy beam^{-1} in USB over a bandwidth of 7.4 GHz in each sideband (excluding the 400 MHz spectral window containing the emission lines). The continuum uv-tables were analyzed in the uv-plane. We find flux densities of 57 ± 14 μJy at 81.2 GHz and 87 ± 14 μJy at 94 GHz, with both measurements consistent with point sources (Table 1). Deconvolution using natural weighting leads to a synthesized beam of 3.1 × 2.2 arcsec^2 (PA = 30°) in LSB and 2.5 × 1.8 arcsec^2 (PA = 30°) in USB. Cleaning of the image cube was done using the Högbom algorithm without applying any mask.

The CO(6–5) and (7–6) line profiles and velocity-integrated maps were produced by subtracting the continuum in each sideband using uv_subtract (Figure 1). Noise levels are 0.28 mJy beam^{-1} per 74 km s^{-1} channel in LSB and 0.26 mJy beam^{-1} per 63 km s^{-1} channel in USB. We produced an averaged uv-table across the line width for both lines, using the uv_average task within MAPPING, and analyzed the line visibilities. Both lines are consistent with an unresolved source in the uv-plane with fluxes $\mathrm{Sdv}_{\rm CO(6-5)} = 0.44 \pm 0.06$ Jy km s^{-1} and $\mathrm{Sdv}_{\rm CO(7-6)} = 0.40 \pm 0.07$ Jy km s^{-1} (Table 1). Both lines are robustly detected with statistical significance of 7σ and 6σ, respectively. A fit with a Gaussian model gives a marginally resolved source and a lower signal-to-noise ratio in the flux, confirming that the source is unresolved in both transitions.

[13] https://www.iram.fr/IRAMFR/GILDAS/

Table 1
Properties of Pōniuā'ena

R.A.	10:07:58.279
decl.	+21:15:28.932
$z^{(a)}_{\rm [C\,II]}$	7.5149 ± 0.0004
$M^{(a)}_{\rm BH}$ [$M_\odot$]	$(1.5 \pm 0.2) \times 10^9$
$F_{\rm cont,79.2GHZ}$ [μJy]	57 ± 14
$F_{\rm cont,96.4GHZ}$ [μJy]	87 ± 14
$z^{(b)}_{\rm CO}$	7.5149 ± 0.0006
$\mathrm{FWHM}_{\rm CO(6-5)}$ [km s^{-1}]	310 ± 65
$F_{\rm CO(6-5)}$ [Jy km s^{-1}]	0.44 ± 0.06
$L'_{\rm CO(6-5)}$ [K km s^{-1}pc^2]	$(2.1 \pm 0.3) \times 10^{10}$
$L_{\rm CO(6-5)}$ [$L_\odot$]	$(2.2 \pm 0.3) \times 10^8$
$\mathrm{FWHM}_{\rm CO(7-6)}$ [km s^{-1}]	261 ± 47
$F_{\rm CO(7-6)}$ [Jy km s^{-1}]	0.40 ± 0.07
$L'_{\rm CO(7-6)}$ [K km s^{-1}pc^2]	$(1.4 \pm 0.2) \times 10^{10}$
$L_{\rm CO(7-6)}$ [$L_\odot$]	$(2.3 \pm 0.4) \times 10^8$
$F_{\rm [C\,I]}$ [Jy km s^{-1}]	<0.18
L'[C I] [K km s^{-1}pc^2]	$<6 \times 10^9$
L[C I] [$L_\odot$]	$<1.0 \times 10^8$
$M(\mathrm{H}_2)^{(c)}$ [$M_\odot$]	$(2.2 \pm 0.2) \times 10^{10}$
$M_{\rm dust}$ [$M_\odot$]	$(1.7 \pm 0.6) \times 10^8$
GDR $^{(d)}$	130
β	1.77 ± 0.18
SFR $^{(e)}$ [$M_\odot$ yr^{-1}]	98

Note. All fluxes are derived from a fit of the visibilities with a point source model. (*a*) Yang et al. (2020). (*b*) Average of CO 6–5 and 7–6 redshifts. (*c*) Assuming a conversion factor $\alpha_{\rm CO} = 0.8$ $M_\odot$(K km s^{-1} pc^2)$^{-1}$ and assuming a brightness temperature ratio $r_{61} = \mathrm{CO(6-5)/CO(1-0)} = 0.75$ (Weiß et al. 2007; Riechers et al. 2009a; Wang et al. 2019; Li et al. 2020; Yang et al. 2019) (*d*) Gas-to-dust ratio. (*e*) The SFR is computed assuming a dust temperature $T_{\rm dust} = 50$ K (see Section 3) and is corrected by a factor of 50%, taking into account the contribution of the QSO to the dust heating (Duras et al. 2017).

The average redshift derived from CO(6–5) and (7–6) lines is $z_{\rm CO} = 7.5149 \pm 0.0006$, consistent with that derived from the [C II] 158 μm line (Yang et al. 2020). The line widths, derived by fitting a single Gaussian to the spectra, are $\mathrm{FWHM}_{\rm CO(6-5)} = 310 \pm 65$ km s^{-1} and $\mathrm{FWHM}_{\rm CO(7-6)} = 261 \pm 47$ km s^{-1}, consistent within 1σ with the [C II] FWHM (Yang et al. 2020). The line fluxes derived from the Gaussian fit are 0.35 ± 0.08 Jy km s^{-1} for CO(6–5) and 0.36 ± 0.07 Jy km s^{-1} for CO(7–6), both consistent with the uv-plane analysis (Table 1).

The line luminosities are L'CO(6–5) = $(2.1 \pm 0.3) \times 10^{10}$ K km s^{-1}pc^{2}and L'CO(7–6) = $(1.4 \pm 0.2) \times 10^{10}$ K km s^{-1}pc^2 (Carilli & Walter 2013). The [C I](2-1) 370 μm emission line is undetected and we derive a 3σ upper limit on the flux of 0.18 Jy km s^{-1}, or L[C I]$<10^8$ $L_\odot$(Table 1), assuming an unresolved source with FWHM = 350 km s^{-1} (i.e., the average FWHM value measured for the CO lines). A scan of the data cubes did not reveal any other line or continuum emitters.

3. Discussion and Conclusions

We use the CO line detections to provide the first measurement of cold molecular gas reservoirs at redshift

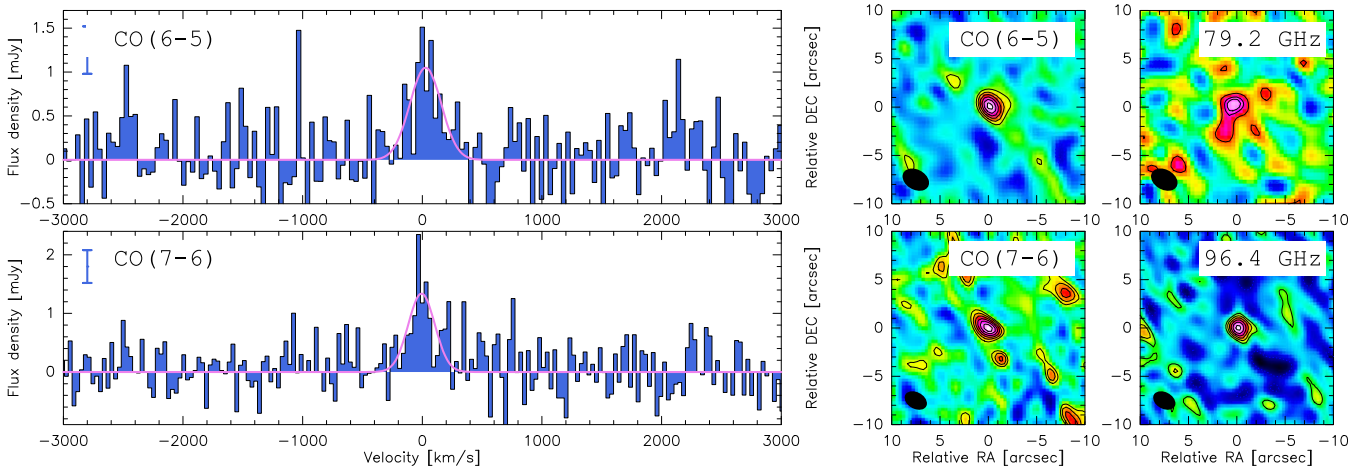

Figure 1. Upper panels: (left to right) the CO(6–5) emission line spectrum, the corresponding velocity-integrated CO map, and the 79.2 GHz continuum map of Pōniuā'ena. Lower panels: the CO(7–6) emission line spectrum, the corresponding velocity-integrated map, and the 96.4 GHz continuum map relative to the phase center set at [R.A.,decl.] = [10:07:58.260, 21:15:29.20]. The velocity zero point is set to the frequency 81.207 GHz for CO(6–5) and 94.734 GHz for CO(7–6). In each panel we report the error bar showing the 1σ error bar in the 10 MHz spectral channel. Magenta lines show the fit with a single Gaussian component; FWHM is reported in Table 1. Contours are drawn starting at 2σ in steps of 1σ ($\sigma = 0.05$ Jy km s^{-1} for CO(6–5), 0.065 Jy km s^{-1} for CO(7–6), 15.5μ Jy for 79.2 GHz continuum, and 12.2μ Jy for 96.4 GHz continuum.

$\sim$7.5 in the host galaxy of quasar Pōniuā'ena. The CO SLED of Pōniuā'ena, limited to the (6–5) and (7–6) transitions, is shown in Figure 2. We show Pōniuā'ena together with other $z > 6$ quasars, and quasar APM 08279+5255 at $z = 3.911$, for which the SLED is well constrained from $J = 2$ up to $J = 17$ (Weiß et al. 2007; Riechers et al. 2009a; Gallerani et al. 2014; Wang et al. 2019; Li et al. 2020). The SLEDs have been normalized to the $J = 6 - 5$ transition. For Pōniuā'ena, the CO SLED shows a flattening at the CO(6–5) and (7–6) transitions, similarly to what is observed in some QSOs at $z \sim 6$, such as J0100+2802, J1148+5251 and J0439+1643 (Riechers et al. 2009b; Yang et al. 2019; Wang et al. 2019). For those quasars, the CO SLED suggests two gas components with $T_{\rm kin} \sim 20$ K and $\sim$150 K (e.g., Yang et al. 2019), and in some cases a contribution from an X-ray-dominated region is required to account for the molecular gas excitation (Gallerani et al. 2014). Detection of CO transitions with $J > 7$ would be needed to constrain the physical conditions in the molecular ISM of Pōniuā'ena.

The main systematic uncertainties in the determination of the molecular mass from CO derive from the CO SLED and the luminosity-to-mass conversion factor, $\alpha_{\rm CO}$. Based on the typical CO SLED of high-redshift quasars (Figure 2), we adopt a line luminosity ratio $r61 = {\rm L'CO(6\text{--}5)/L'CO(1\text{--}0)} = 0.75$, which is the average ratio for $z > 4$ quasars (Weiß et al. 2007; Riechers et al. 2009a; Wang et al. 2019; Li et al. 2020; Yang et al. 2019), and a conversion factor $\alpha_{\rm CO} = 0.8\,M_\odot$ (K km s^{-1} pc^2)$^{-1}$ (Carilli & Walter 2013) to derive the molecular gas mass from the CO(6–5) line luminosity. With these assumptions we find a molecular mass $M({\rm H_2}) = \alpha_{\rm CO} \times L'CO(6\text{–}5)/r61 = (2.2 \pm 0.2) \times 10^{10}\ M_\odot$. If instead we used the CO excitation template of $z \sim 2.5$ galaxies in ASPECS, which is less steep than that of typical quasars and which has $r61 = 0.28$ or equivalently $r71 = {\rm L'CO(7\text{–}6)/L'CO(1\text{–}0)} = 0.17$ (Boogaard et al. 2020; Decarli et al. 2022), this would imply a larger molecular mass by a factor of $\sim$3.

Applying the relation by Zanella et al. (2018) to convert the [C II] luminosity (Yang et al. 2020) into molecular mass would yield $M({\rm H_2[C\,II]}) \sim 5.7 \times 10^{10}\ M_\odot$. Our fiducial value, $M({\rm H_2}) = (2.2 \pm 0.2) \times 10^{10}\ M_\odot$, is at the lowest end of the range found for $z > 6$ quasars, and the luminosity ratio for Pōniuā'ena is L[C II]/L CO(7–6) = 7, while the mean value for $z > 6$ quasars is around 20 (Feruglio et al. 2018; Wang et al. 2019; Decarli et al. 2022). Pōniuā'ena appears to be a H_2-rich system as it hosts at least $\times$5 a larger molecular gas reservoir compared to the $z \sim 7.5$ J1342+0928 (Pisco) quasar (Novak et al. 2019) for the same [C II] luminosity.

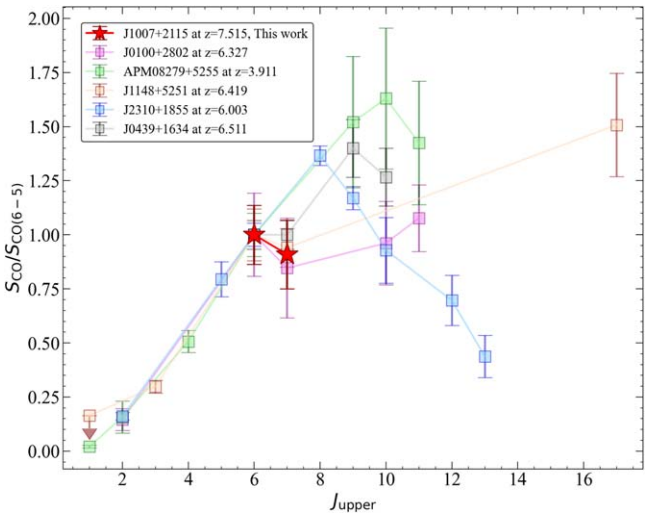

Figure 2. CO SLED of Pōniuā'ena compared with those of other QSOs at lower redshift. The CO SLED for Pōniuā'ena is shown as red stars, for J0439 +1634 at $z = 6.511$ as gray squares (Yang et al. 2019), for J1148+5251 at $z = 6.419$ as orange squares (Riechers et al. 2009a; Gallerani et al. 2014), for J0100+2802 at $z = 6.327$ as purple squares (Wang et al. 2019), for J2310 +1855 at $z = 6.003$ as blue squares (Li et al. 2020), and for APM 08279+5255 at $z = 3.911$ as green squares (Papadopoulos et al. 2001; Weiß et al. 2007).

The dynamical mass of the system cannot be derived because the source is unresolved in both CO and [C II]. A rough estimate of the total dynamical mass of the system can be described by $M_{\rm dyn} \approx M({\rm H_2}) + M({\rm H\,I}) + {\rm M_{BH}}$, where M(H I) is the atomic gas mass associated with photodissociation regions and derived from [C II], $M({\rm H\,I}) = 1.44 \times 10^9\ M_\odot$ (Hailey-

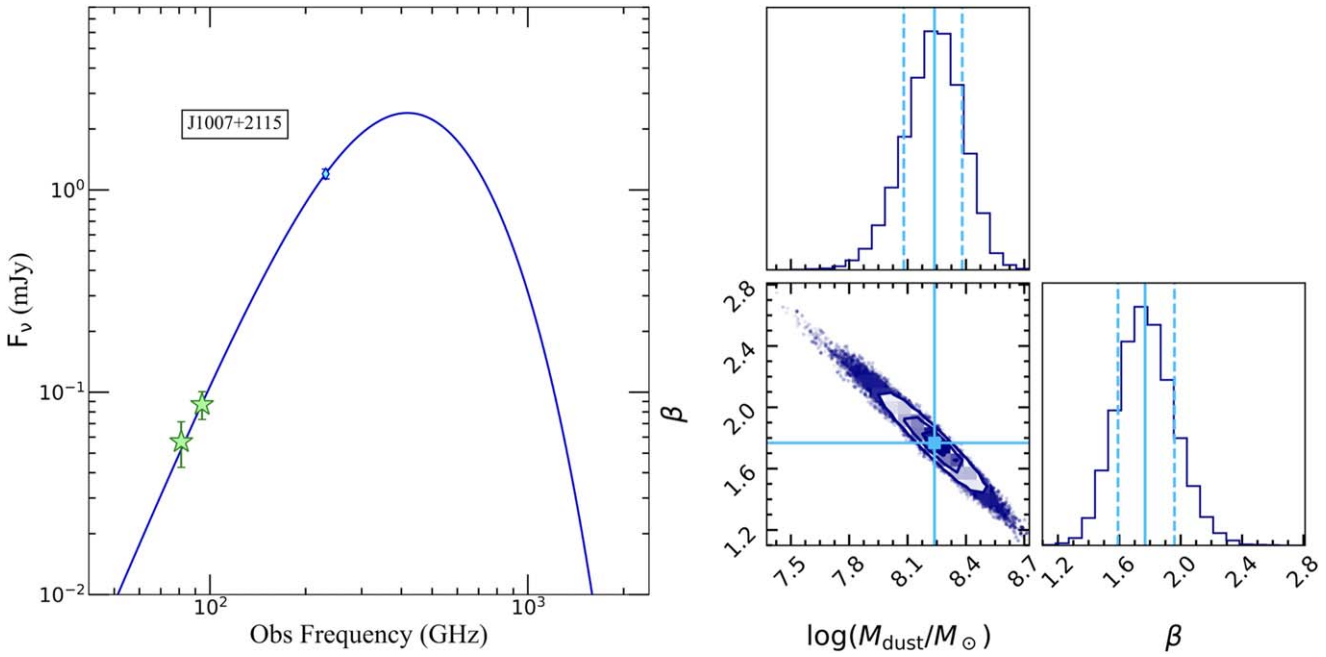

Figure 3. Results of the SED fitting of Pōniuā'ena. Left panel: SED using our new NOEMA data at 3 mm (i.e., ∼80 and ∼90 GHz; green stars) and the ALMA data at ∼230 GHz taken from Yang et al. (2020; cyan diamond). The best-fitting curve with dust temperature fixed at 50 K is shown as a solid blue line. Right panels: corner plot showing the two-dimensional posterior probability distributions of $M_{\rm dust}$, β. Cyan solid lines indicate the best-fitting parameter, while the dashed lines mark the 16th and 84th percentiles for each parameter.

Dunsheath et al. 2010) and $M_{\rm BH}$ is the black hole mass from Yang et al. (2020), and we neglect the stellar and dark matter components. We find $M_{\rm dyn} \sim 2.7 \times 10^{10}\,M_\odot$, where the molecular mass fraction is $M({\rm H_2})/M_{\rm dyn} \sim 80\%$. Should the stellar component be significantly massive, as discussed in Valiante et al. (2014), the gas fraction would decrease to $\lesssim$40%. A more accurate estimate of the dynamical mass would require [C II] or CO observations that spatially resolve the host galaxy.

The spectral energy distribution (SED) of the cold dust component of Pōniuā'ena, based on these observations and ALMA Band 6 observations from Yang et al. (2020), is shown in Figure 3. We model the dust continuum with a modified blackbody function given by

$$S^{\rm obs}_{\nu_{\rm obs}} = \frac{\Omega}{(1+z)^3}[B_\nu(T_{\rm dust}(z)) - B_\nu(T_{\rm CMB}(z))](1 - e^{-\tau_\nu}), \quad (1)$$

where $\Omega = (1+z)^4 A_{\rm gal} D_{\rm L}^{-2}$ is the solid angle with $A_{\rm gal}$, the surface area, and where $D_{\rm L}$ is the luminosity distance of the galaxy, respectively. The dust optical depth is given by $\tau_\nu = \frac{M_{\rm dust}}{A_{\rm galaxy}} k_0 \left(\frac{\nu}{250\ {\rm GHz}}\right)^\beta$, with β the emissivity index and $k_0 = 0.45\ {\rm cm^2\ g^{-1}}$ the mass absorption coefficient (Beelen et al. 2006). The effect of the CMB on the dust temperature is taken into account as $B_\nu(T_{\rm CMB}(z) = T_0(1+z))$ (da Cunha et al. 2013), with $T_0 = 2.73$ K. Since the source is unresolved, the adopted area of the galaxy is the dust size commonly found in high-z QSOs (Shao et al. 2022; Tripodi et al. 2022; Walter et al. 2022), which is $0\farcs2 \times 0\farcs2$, corresponding to $\sim 1.0 \times 1.0\ {\rm kpc^2}$ at the rest frame of our source.

Dust temperature cannot be constrained with the low-frequency data in hand; hence we fix it to $T_{\rm dust} = 50$ K. This may be considered the median value in $z = 6-7$ quasars, for which a range in dust temperature of 30 to 70 K is found (Leipski et al. 2014; Schneider et al. 2015; Carniani et al. 2019; Wang et al. 2019; Tripodi et al. 2023, 2022). We explore the two-dimensional parameter space using a Markov Chain Monte Carlo algorithm implemented in the EMCEE package (Foreman-Mackey et al. 2013), assuming uniform priors for $M_{\rm dust}$ and β. We derive a cold dust mass of $M_{\rm dust} = (1.7 \pm 0.6) \times 10^8\,M_\odot$ and a dust emissivity index of $\beta = 1.77 \pm 0.18$. The dust mass in Pōniuā'ena is in agreement with the median dust mass found in quasars at $z = 6$–6.6 (Venemans et al. 2018). Varying the temperature up to $T_{\rm dust} = 70$ K, the dust mass and emissivity index both decrease to $M_{\rm dust} = 1.4 \times 10^8\,M_\odot$ and $\beta = 1.41$, respectively.

The gas-to-dust ratio (GDR) is about ∼130, in line with quasars at lower redshift (Bischetti et al. 2021; Tripodi et al. 2022), and remarkably consistent even with the Milky Way (135; Jones et al. 2017) and local values (Dunne et al. 2021). We compute the SFR using the relation by Kennicutt (1998) scaled to a Chabrier initial mass function: SFR $(M_\odot\ {\rm yr^{-1}}) = 10^{-10}\,L^{\rm IR}_{8-1000\mu{\rm m}}(L_\odot)$. We also take into account the contribution of the luminous QSO to the dust heating with a factor of 50% (Duras et al. 2017), and we obtain SFR ∼100 $M_\odot\ {\rm yr^{-1}}$, in agreement with the broad range suggested by Yang et al. (2020). By using the [C II] line detection and a single continuum measurement at 231 GHz and assuming $T_{\rm dust} = 47$ K and $\beta = 1.6$, they found an SFR in the range 80–700 $M_\odot\ {\rm yr^{-1}}$. However, this value has a large systematic uncertainty since the dust temperature is not determined. At face value this would imply a star formation efficiency (SFE) of ${\rm SFE} = {\rm SFR}/{\rm M(H_2)} = 4.4 \times 10^{-9}\ {\rm yr^{-1}}$. Observations in ALMA Band 9 are needed to possibly resolve the host galaxy and tightly constrain both $T_{\rm dust}$ and SFR (Tripodi et al. 2023).

Pōniuā'ena, together with J1342+0928 and J1120+0641, belong to the HYPERION sample of quasars powered by SMBHs, which experienced the fastest mass growth among luminous $z > 6$ quasars (Zappacosta et al. 2023). In order to

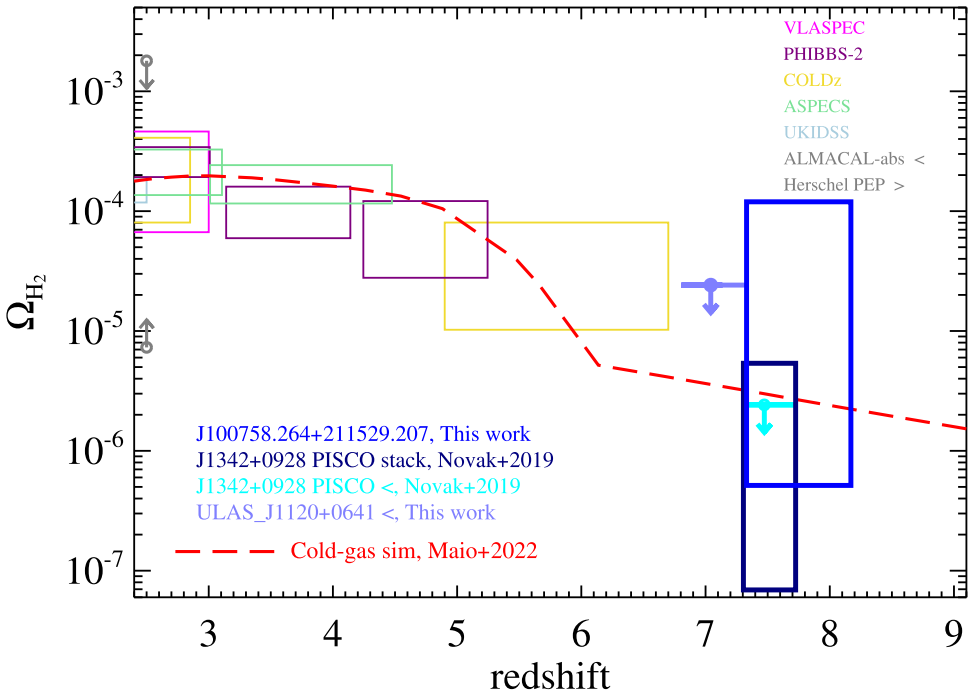

Figure 4. Comoving cosmic mass density of cold molecular gas as a function of redshift. Vertical sizes indicate the uncertainties in each bin. Data are from Riechers et al. (2020a, 2020b; VLASPEC, COLDz), Decarli et al. (2020; ASPECS), Lenkić et al. (2020; PHIBSS-2), Garratt et al. (2021; UKIDSS-UDS), and Hamanowicz et al. (2023; ALMACAL-CO), and upper/lower limits from ALMACAL-abs (Klitsch et al. 2019) and Herschel PEP (Berta et al. 2013). Theoretical expectation from cold-gas simulations (dashed line) are by Maio et al. (2022).

grow their $\gtrsim 10^9\ M_\odot$ SMBH, these quasars would require a black hole seed of $10^4\ M_\odot$ under the assumption of continuous accretion at the Eddington rate or a series of short active bursts of super-Eddington accretion starting from lower-mass seeds. The CO upper limits in J1342+0928 and J1120+0641 suggest that the fast SMBH growth rate in these quasars does not seem to be directly related to the molecular reservoir's buildup in the host galaxies. Alternatively, some different combination of both Eddington-limited massive seed and super-Eddington accretion growth pathways may affect their ISM properties differently, allowing for some degree of symbiotic SMBH/host galaxy growth (Volonteri 2012). To better investigate this, we are planning a follow-up investigation of the molecular reservoirs in all HYPERION quasars.

Finally, we derive an estimate of the cosmic mass density of molecular mass, Ω_{H_2}, at $z \sim 7.5$. Thanks to the wide band covered by our observation, we probe the redshift range between 7.33 and 8.17, or the range 600–700 Myr of cosmic time; the field of view is taken as the primary beam of the observation, about 50″. We use the estimated molecular mass $M(H_2)$ in the corresponding cosmic volume, V, to derive the H_2 mass density parameter $\Omega_{H_2} = M(H_2)/\ V\ /\rho_{\rm crit,\ 0}$, where $\rho_{\rm crit,\ 0} \simeq 277.4\ h^2\ M_\odot\ {\rm kpc}^{-3}$ is the present-day cosmological critical density and $h = H_0/(100\ {\rm km\ s^{-1}\ Mpc^{-1}})$.

Figure 4 shows the Ω_{H_2} redshift evolution derived from this observation and those of two other quasars at $z > 7$ for which CO upper limits are measured, i.e., J1342+0928 (for which we also report the tentative stack detection by Novak et al. 2019), and ULAS J1120+0641 (ALMA archive). Literature values at lower z are from VLASPEC, COLDz (Riechers et al. 2020a, 2020b), ASPECS (Decarli et al. 2020), PHIBSS-2 (Lenkić et al. 2020), UKIDSS-UDS (Garratt et al. 2021), and ALMACAL-CO (Hamanowicz et al. 2023), and upper and lower limits are from ALMACAL-abs (Klitsch et al. 2019) and Herschel PACS Evolutionary Probe (PEP; Berta et al. 2013). The value inferred by our analysis of Pōniuā'ena is $\Omega_{H_2} \simeq 1.31 \times 10^{-5}$. Upper and lower limits are evaluated by considering a statistical error on H_2 mass determination of $0.16 \times 10^{10}\ M_\odot$, a systematic calibration error of 10%, and CO SLED lower and upper errors of 0.65 and $5.94 \times 10^{10}\ M_\odot$. For J1342+0928 (Novak et al. 2019) the resulting upper limit between $z \simeq 7.30$ and 7.72 suggests $\Omega_{H_2} < 2.42 \times 10^{-6}$, while the stacking analysis gives $\Omega_{H_2} \simeq 1.13 \times 10^{-6}$. In this latter case, a statistical error on the H_2 mass of $2.2 \times 10^8\ M_\odot$ and an upper limit of a factor of 2 for the stacking error have been considered. The ALMA archival observation of ULAS J1120+0641 allows us to estimate an Ω_{H_2} upper limit of 2.42×10^{-5} at $z \simeq 6.80$–7.13.

As a comparison, we also show the trend expected by the latest, accurate, nonequilibrium molecular-chemistry cosmological simulations of cold gas at early times by Maio et al. (2022). The predicted Ω_{H_2} behavior at $z > 6$ is mainly driven by H_2 formation via the H^- channel since in the simulation the dust growth is inefficient at such primordial epochs. At later times the effects of UV radiation (that enhances production of free charges at temperatures around or below 10^4 K) and dust grain catalysis in progressively enriched media boost Ω_{H_2} expectations. Overall, the values we find are in line with the general trend suggested by literature estimates at $z < 7$ and agree fairly well with the latest theoretical expectations. Although Ω_{H_2} determinations by quasar data might be slightly biased, as individual objects do not necessarily represent a fair sample of the universe, our results suggest that it is possible to leverage on this by combining different objects at similar cosmological epochs. We note that this work represents the first attempt to set constraints on H_2 abundances by combining state-of-the-art interferometric observations of the cold dense molecular gas in the first 700 Myr with state-of-the-art cold-gas

modeling. Previous works (e.g., Abel et al. 1997; Maio et al. 2007) have indeed either neglected a fully complete modeling of primordial molecules or could not rely on constraints from observational data for the early regimes probed here.

Acknowledgments

This publication has received funding from the European Union's Horizon 2020 research and innovation program under grant agreement No. 101004719 (ORP). Authors acknowledge financial support from PRIN MIUR contract 2017PH3WAT; PRIN MAIN STREAM INAF "black hole winds and the baryon cycle"; the Horizon 2020 INFRAIA Programme under grant Agreement No. 871158 AHEAD2020; INAF Large Grant 2022 "Toward an holistic view of the Titans: multi-band observations of $z > 6$ QSOs powered by greedy supermassive black holes." This work is co-funded by the European Union (ERC, WINGS, 101040227). Views and opinions expressed are, however, those of the author(s) only and do not necessarily reflect those of the European Union or the European Research Council Executive Agency. Neither the European Union nor the granting authority can be held responsible for them. This work is based on observations carried out under project number W21ED with the IRAM NOEMA Interferometer. IRAM is supported by INSU/CNRS (France), MPG (Germany) and IGN (Spain). This paper makes use of the following ALMA data: ADS/JAO.ALMA#2019.1.01025.S. ALMA is a partnership of ESO (representing its member states), NFS (USA) and NINS (Japan), together with NRC (Canada), MOST and ASIAA (Taiwan) and KASI (Republic of Korea), in cooperation with the Republic of Chile. The Joint ALMA Observatory is operated by ESO, AUI/NRAO and NAOJ.

ORCID iDs

Chiara Feruglio https://orcid.org/0000-0002-4227-6035
Umberto Maio https://orcid.org/0000-0002-0039-3102
Roberta Tripodi https://orcid.org/0000-0002-9909-3491
Jan Martin Winters https://orcid.org/0000-0001-6114-9173
Luca Zappacosta https://orcid.org/0000-0002-4205-6884
Manuela Bischetti https://orcid.org/0000-0002-4314-021X
Francesca Civano https://orcid.org/0000-0002-2115-1137
Stefano Carniani https://orcid.org/0000-0002-6719-380X
Valentina D'Odorico https://orcid.org/0000-0003-3693-3091
Fabrizio Fiore https://orcid.org/0000-0002-4031-4157
Simona Gallerani https://orcid.org/0000-0002-7200-8293
Michele Ginolfi https://orcid.org/0000-0002-9122-1700
Roberto Maiolino https://orcid.org/0000-0002-4985-3819
Enrico Piconcelli https://orcid.org/0000-0001-9095-2782
Rosa Valiante https://orcid.org/0000-0003-3050-1765
Maria Vittoria Zanchettin https://orcid.org/0000-0001-7883-496X

References

Abel, T., Anninos, P., Zhang, Y., & Norman, M. L. 1997, NewA, 2, 181
Bañados, E., Venemans, B. P., Mazzucchelli, C., et al. 2018, Natur, 553, 473
Beelen, A., Cox, P., Benford, D. J., et al. 2006, ApJ, 642, 694
Berta, S., Lutz, D., Nordon, R., et al. 2013, A&A, 555, L8
Bischetti, M., Feruglio, C., Piconcelli, E., et al. 2021, A&A, 645, A33
Boogaard, L. A., van der Werf, P., Weiss, A., et al. 2020, ApJ, 902, 109
Carilli, C. L., & Walter, F. 2013, ARA&A, 51, 105
Carniani, S., Gallerani, S., Vallini, L., et al. 2019, MNRAS, 489, 3939
da Cunha, E., Groves, B., Walter, F., et al. 2013, ApJ, 766, 13
Decarli, R., Aravena, M., Boogaard, L., et al. 2020, ApJ, 902, 110
Decarli, R., Pensabene, A., Venemans, B., et al. 2022, A&A, 662, A60
Dunne, L., Maddox, S. J., Vlahakis, C., & Gomez, H. L. 2021, MNRAS, 501, 2573
Duras, F., Bongiorno, A., Piconcelli, E., et al. 2017, A&A, 604, A67
Fan, X., Narayanan, V. K., Lupton, R. H., et al. 2001, AJ, 122, 2833
Feruglio, C., Fiore, F., Carniani, S., et al. 2018, A&A, 619, A39
Foreman-Mackey, D., Hogg, D. W., Lang, D., & Goodman, J. 2013, PASP, 125, 306
Gallerani, S., Ferrara, A., Neri, R., & Maiolino, R. 2014, MNRAS, 445, 2848
Garratt, T. K., Coppin, K. E. K., Geach, J. E., et al. 2021, ApJ, 912, 62
Hailey-Dunsheath, S., Nikola, T., Stacey, G. J., et al. 2010, ApJL, 714, L162
Hamanowicz, A., Zwaan, M. A., Péroux, C., et al. 2023, MNRAS, 519, 34
Jones, A. P., Köhler, M., Ysard, N., Bocchio, M., & Verstraete, L. 2017, A&A, 602, A46
Kennicutt, R. C. J. 1998, ARA&A, 36, 189
Klitsch, A., Péroux, C., Zwaan, M. A., et al. 2019, MNRAS, 490, 1220
Leipski, C., Meisenheimer, K., Walter, F., et al. 2014, ApJ, 785, 154
Lenkić, L., Bolatto, A. D., Förster Schreiber, N. M., et al. 2020, AJ, 159, 190
Li, J., Wang, R., Riechers, D., et al. 2020, ApJ, 889, 162
Maio, U., Dolag, K., Ciardi, B., & Tornatore, L. 2007, MNRAS, 379, 963
Maio, U., Péroux, C., & Ciardi, B. 2022, A&A, 657, A47
Maiolino, R., Cox, P., Caselli, P., et al. 2005, A&A, 440, L51
Mazzucchelli, C., Bañados, E., Venemans, B. P., et al. 2017, ApJ, 849, 91
Novak, M., Bañados, E., Decarli, R., et al. 2019, ApJ, 881, 63
Onoue, M., Kashikawa, N., Matsuoka, Y., et al. 2019, ApJ, 880, 77
Papadopoulos, P., Ivison, R., Carilli, C., & Lewis, G. 2001, Natur, 409, 58
Pensabene, A., Decarli, R., Bañados, E., et al. 2021, A&A, 652, A66
Riechers, D. A., Boogaard, L. A., Decarli, R., et al. 2020a, ApJL, 896, L21
Riechers, D. A., Hodge, J. A., Pavesi, R., et al. 2020b, ApJ, 895, 81
Riechers, D. A., Walter, F., Bertoldi, F., et al. 2009b, ApJ, 703, 1338
Riechers, D. A., Walter, F., Carilli, C. L., & Lewis, G. F. 2009a, ApJ, 690, 463
Schneider, R., Bianchi, S., Valiante, R., Risaliti, G., & Salvadori, S. 2015, A&A, 579, A60
Shao, Y., Wang, R., Weiss, A., et al. 2022, A&A, 668, A121
Tripodi, R., Feruglio, C., Fiore, F., et al. 2022, A&A, 665, A107
Tripodi, R., Feruglio, C., Kemper, F., et al. 2023, ApJL, 946, L45
Valiante, R., Schneider, R., Salvadori, S., & Gallerani, S. 2014, MNRAS, 444, 2442
Venemans, B. P., Decarli, R., Walter, F., et al. 2018, ApJ, 866, 159
Venemans, B. P., Walter, F., Decarli, R., et al. 2017, ApJ, 837, 146
Venemans, B. P., Walter, F., Neeleman, M., et al. 2020, ApJ, 904, 130
Volonteri, M. 2012, Sci, 337, 544
Walter, F., Carilli, C., Bertoldi, F., et al. 2004, ApJL, 615, L17
Walter, F., Neeleman, M., Decarli, R., et al. 2022, ApJ, 927, 21
Wang, F., Wang, R., Fan, X., et al. 2019, ApJ, 880, 2
Wang, F., Wu, X.-B., Fan, X., et al. 2016, ApJ, 819, 24
Wang, F., Yang, J., Fan, X., et al. 2021, ApJL, 907, L1
Wang, R., Wagg, J., Carilli, C. L., et al. 2013, ApJ, 773, 44
Weiß, A., Downes, D., Neri, R., et al. 2007, A&A, 467, 955
Willott, C. J., Delorme, P., Reylé, C., et al. 2010, AJ, 139, 906
Yang, J., Venemans, B., Wang, F., et al. 2019, ApJ, 880, 153
Yang, J., Wang, F., Fan, X., et al. 2020, ApJL, 897, L14
Yue, M., Yang, J., Fan, X., et al. 2021, ApJ, 917, 99
Zanella, A., Daddi, E., Magdis, G., et al. 2018, MNRAS, 481, 1976
Zappacosta, L., Piconcelli, E., Fiore, F., et al. 2023, arXiv:2305.02347